Supplemental Material: *Ab initio* prediction of a negative Barkas coefficient for slow protons and antiprotons in LiF

Xixi Qi and Fabien Bruneval
Université Paris-Saclay, CEA, Service de Recherches de Métallurgie Physique, F-91191 Gif-sur-Yvette, France

Ivan Maliyov
Department of Applied Physics and Materials Science,
California Institute of Technology, Pasadena, California 91125, USA

In the Supplemental Material, we provide additional data about the robustness of our RT-TDDFT calculations that predict a negative Barkas coefficient in the electronic stopping power of LiF. We also describe how we include the classical nuclear stopping power. We finally give an illustrative example for the F^- collision problem.

I. ELECTRONIC STOPPING POWER BASED ON CLUSTER CALCULATIONS

A. Convergence of the impact parameter quadrature in random electronic stopping power

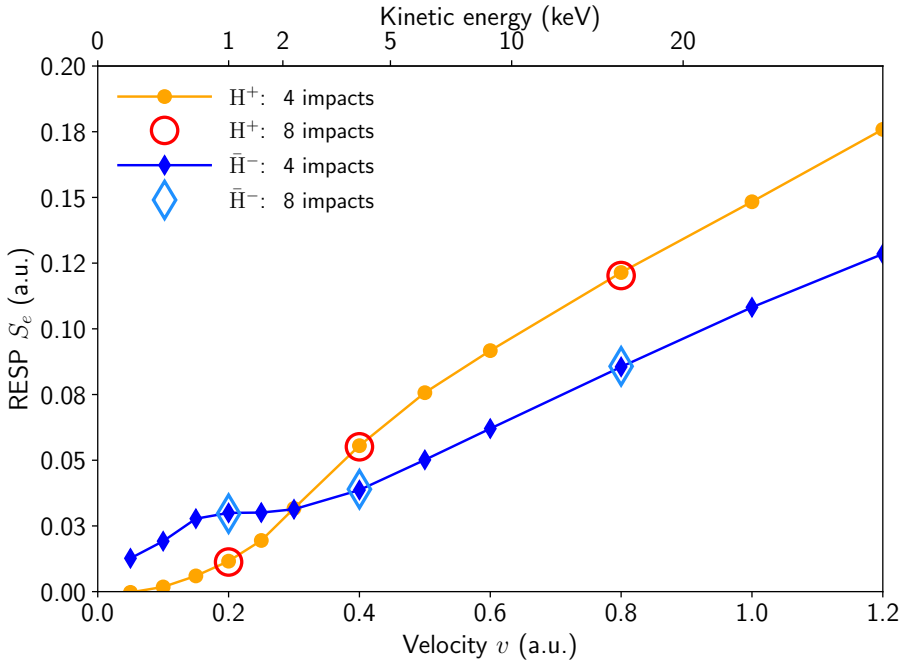

FIG. 1. Convergence with respect to the impact parameter discretization for the calculated LiF RESP of protons and antiprotons.

Labeling the velocity direction z, the random electronic stopping power (RESP) is an average over all the possible impact parameters in the xy plane.

In the present work focusing on the $\langle 111 \rangle$ direction, we assume a polar symmetry around the central atomic column. Therefore, we selected 4 and 8 impact parameters along a single line in the xy plane. Then the RESP is obtained with a quadrature with the proper geometrical weights to account for the polar symmetry, as described in Ref. 1

Figure 1 shows the very good convergence reached with only 4 impact points. We have selected a given representative line in the xy plane in order to save computational resources. This simplification is valid for the direction $\langle 111 \rangle$. A different direction will be discussed in the next subsection.

B. Independence of the RESP with respect to the velocity direction

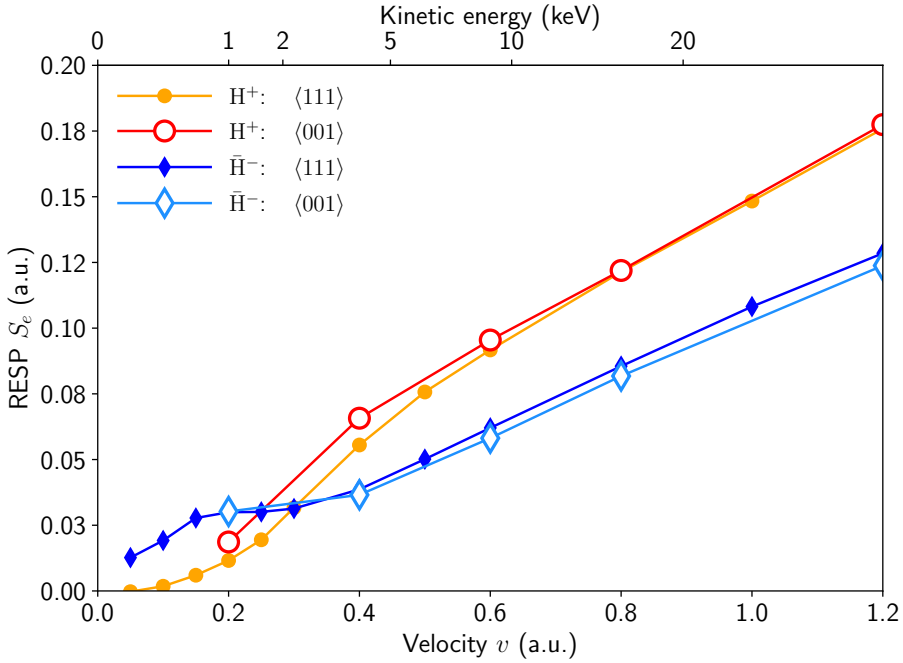

FIG. 2. Direction dependence of the calculated LiF RESP for protons and antiprotons for two velocity directions.

Here we study the direction dependence of the RESP in LiF. We compare our original LiF $\langle 111 \rangle$-oriented 126-atom cluster to a $\langle 001 \rangle$-oriented 144-atom cluster. Of course, changing the orientation forced us to slightly change the cylindrical cluster, but we kept the length and radius of the clusters as similar as possible.

Figure 2 shows a good agreement of the RESP evaluated for the $\langle 111 \rangle$ and the $\langle 001 \rangle$ orientations. We noticed that the $\langle 001 \rangle$ direction does not respect the polar symmetry as well as the $\langle 111 \rangle$ direction. In the $\langle 001 \rangle$ orientation, the polar symmetry mentioned above is broken, especially for proton at low velocity. As a consequence, the $\langle 001 \rangle$ results reported in Fig. 2 were obtained with a complete 2D quadrature in the xy-plane. In practice, we find that 9 impact parameters in the xy-plane are sufficient for a good quadrature.

The agreement between the two directions justifies our choice of the sole $\langle 111 \rangle$ direction in our study.

C. Convergence with respect to the cluster size

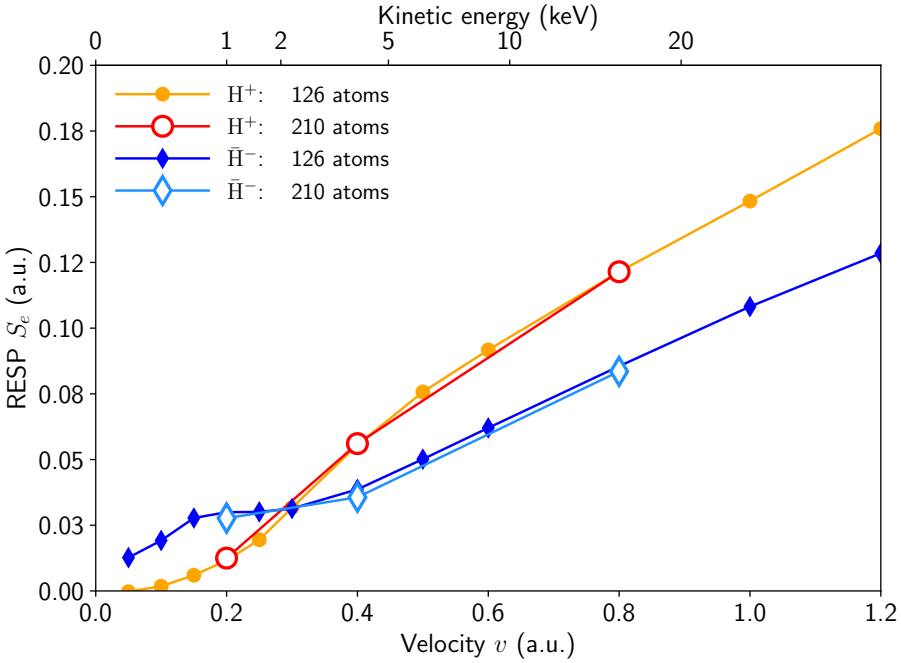

FIG. 3. Cluster radius dependence of the calculated LiF RESP for protons and antiprotons.

Our methodology evaluates the RESP of the periodic solids using a finite cylindrical cluster. This model finds its justification in the local nature of the electronic excitations induced by the traveling ion. Here, we check the validity of this model in practice.

Figure 1 of the Letter shows that the electronic energy variation $E(z) - E(z-a)$ on a periodicity length a reaches a stationary value on a wide range of depth z. The convergence on the length of the cylindrical cluster is then already granted.

In Fig. 3, we compare the RESP for two clusters with two different radii. The results for the original cluster comprising 126 atoms agree very well with a larger cluster of 210 atoms.

D. Independence of the RESP with respect to the exchange-correlation functional

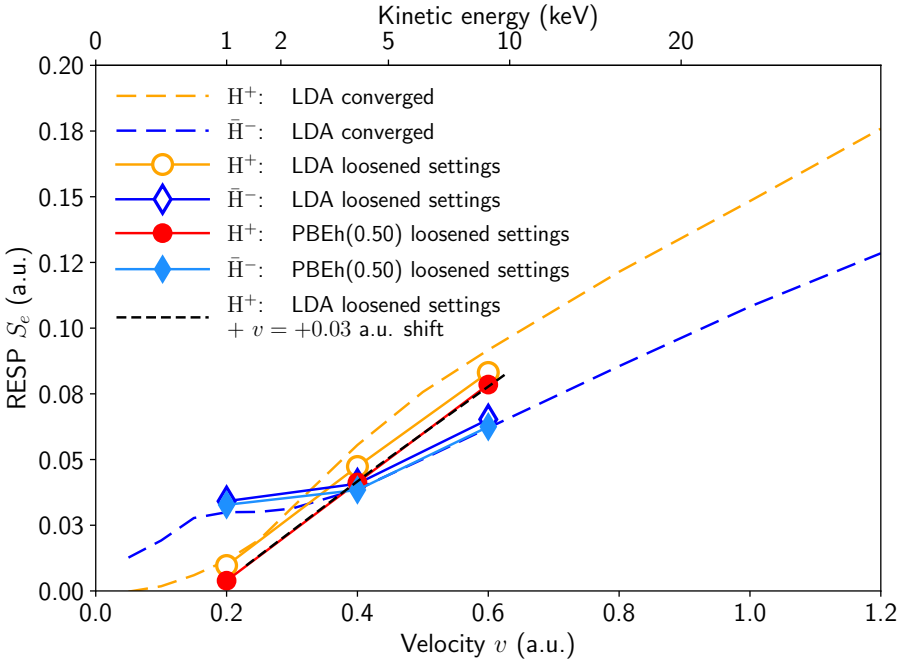

FIG. 4. Effect of the exchange-correlation functional on the calculated LiF RESP for protons and antiprotons. We employ LDA and a hybrid functional, PBEh(0.50). Here, due to a large computational cost, we use loosened settings for the basis and the cluster size (see text). Shifting the LDA proton curve by +0.03 a.u. (dashed black line) reproduces the PBEh(0.50) proton curve.

As already mentioned in several earlier studies[1–3], the exchange-correlation functional of TDDFT has little effect on the stopping power. However, in the specific cases of antiprotons or low-velocities, it is not fully assessed yet.

Here we select two approximate adiabatic functionals: LDA and PBEh(0.50). PBEh(0.50) is a tuned hybrid functional that mixes 50 % of Fock exchange together with 50 % of PBE exchange. Full PBE correlation is included. We selected this specific hybrid functional with a large amount of Fock exchange (compared to the 25 % contained in PBE0) because it should be more realistic for a wide band gap insulator like LiF for which we know PBE0 underestimates the band gap[4].

Hybrid functionals are known to be able to capture the effect of electron-hole pairs (excitons)[5]. PBEh(0.50) will help us to determine whether those effects are indeed important. The calculation of the Fock exchange contained in PBEh(0.50) is time-consuming. Therefore we reduced the calculation parameters: we used a 84-atom cluster instead of 126 (by decreasing the radius of the cylindrical cluster). The central atoms are described with the `aug-cc-pVTZ` basis set instead of `aug-cc-pCVQZ`.

Figure 4 shows the limited effect of the approximate functional on RESP. The antiproton curves are very much insensitive to the exchange-correlation approximation, whereas there exists only a small shift of $v = 0.03$ a.u. between the LDA proton curve and the PBEh(0.50) one.

Reducing the basis set and the cluster size did not affect the overall shape of the curves as shown by the comparison with the fully converged LDA results. Therefore, the loosened settings are representative to the converged results.

II. NUCLEAR STOPPING POWER

The total stopping power can be decomposed in electronic and nuclear contributions:

$$S(v) = S_e(v) + S_n(v). \tag{1}$$

While S_e involves the complicated treatment of the electronic excitations, S_n originates from the classical collision between the ionic projectile and the target nucleus. In this study, we have obtained $S_e(v)$ from fixed-atom TDDFT trajectories. This procedure is well documented in several reviews[3,6].

A. Evaluation of S_n for antiprotons in LiF

Here, we describe the evaluation of the S_n contribution. The binary collision approximation (BCA) has been used for years with great success to evaluate S_n[7,8]. In particular, S_n for proton in LiF can be obtained from SRIM code and from papers[7,8].

However, much less information is available for antiproton projectiles. Hereafter we follow step-by-step the BCA approach by Nordlund *et al.*[9] in order to obtain the nuclear stopping cross-section (S_n/ρ) of Li and F, which were not treated by Nordlund and coworkers.

First, we evaluated with MOLGW[10] the quantum-mechanical energy versus bond length $E(r)$ of an antiproton and the target atom (Li or F). The energy is obtained within MP2 and using the `aug-cc-pCVTZ` basis for the atom and the `aug-cc-pVTZ` basis of hydrogen for the antiproton. We have checked that the results are very little sensitive to the basis and to electronic structure method.

The screening function $\phi(r)$ is implicitly defined (in atomic units) as

$$E(r) = \frac{Z_1 Z_2}{r}\phi(r). \tag{2}$$

It measures the ratio between the total energy and the nuclear Coulomb repulsion. $\phi(r)$ tends to 1 when r goes to zero (no screening).

Second, for computational speed purposes, we fit $\phi(r)$ with a sum of exponential fucntions:

$$\phi(r) = b_1 \exp(-a_1 r) + b_2 \exp(-a_2 r) + b_3 \exp(-a_3 r). \tag{3}$$

The fitted coefficients are given below.

	a_1 Å^{-1}	a_2 Å^{-1}	a_3 Å^{-1}	b_1	b_2	b_3
Li	5.14054	0.50872	–	0.66028	0.33972	–
F	30.3607	3.23009	0.502386	0.12485	0.85683	0.01831

Third, series of classical Newtonian calculations of the binary collision are performed to numerically obtain the stopping cross-section:

$$\frac{S_n(v)}{\rho} = \int_0^{+\infty} dp 2\pi p \Delta E(v,p), \tag{4}$$

where $\Delta E(v,p)$ is the kinetic energy loss of the projectile during the collision.

In Fig. 5, we show the nuclear stopping cross-section (S_n/ρ) for different atoms. Our results for Si agree very well with Nordlund *et. al.*[9], validating our numerical implementation. The new results for Li and F are consistent with the neighboring elements (Be and O extracted from Ref. 9).

The stopping power of proton in Li and F, as obtained with the famous ZBL universal potential[7], are shown for comparison. We conclude in agreement with Nordlund and coworkers that the nuclear stopping power of antiprotons is noticeably larger than that of protons.

Finally, the stopping power for LiF is obtained within the BCA, assuming the Bragg additivity law[7]:

$$S_n^{\mathrm{LiF}}(v) = \rho_{\mathrm{LiF}} \left[\left(\frac{S_n}{\rho}\right)^{\mathrm{Li}} + \left(\frac{S_n}{\rho}\right)^{\mathrm{F}} \right]. \tag{5}$$

The final results for S_e, S_n, and the total stopping power are reported in Fig. 6. The nuclear stopping power becomes non-negligible below $v = 0.2$ au, but as first noted by Nordlund and coworkers, the nuclear stopping power of the antiproton is larger than that of the proton, which finally increases even further the negative Barkas coefficient.

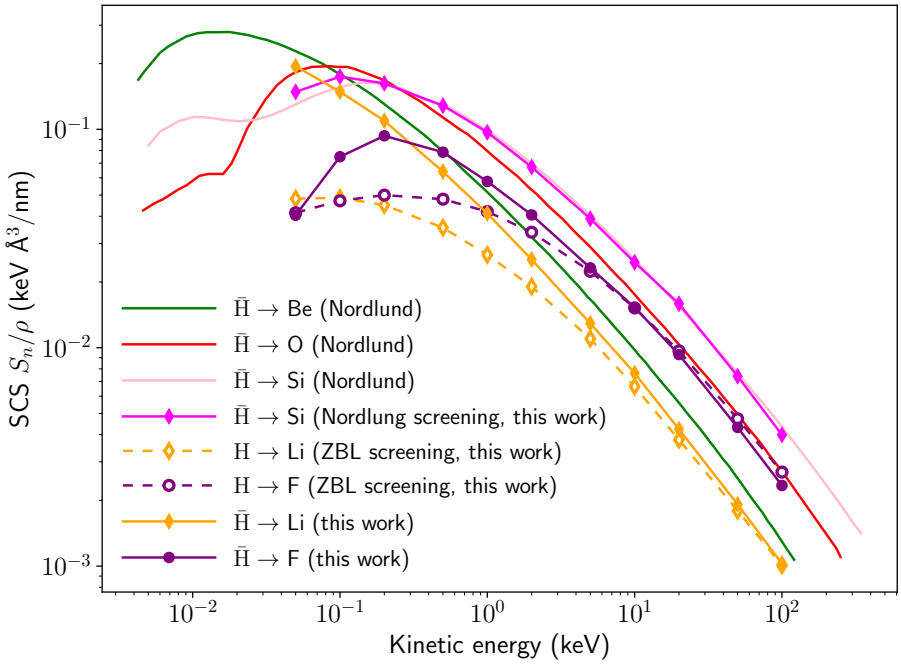

FIG. 5. Nuclear stopping cross-section (S_n/ρ) for the collision between an antiproton and an atom of Be, O, Si (from Ref. 9), Si, Li, F (from this work). Collision of a proton with Li and F using ZBL screened potential is also shown for comparison (dahsed lines).

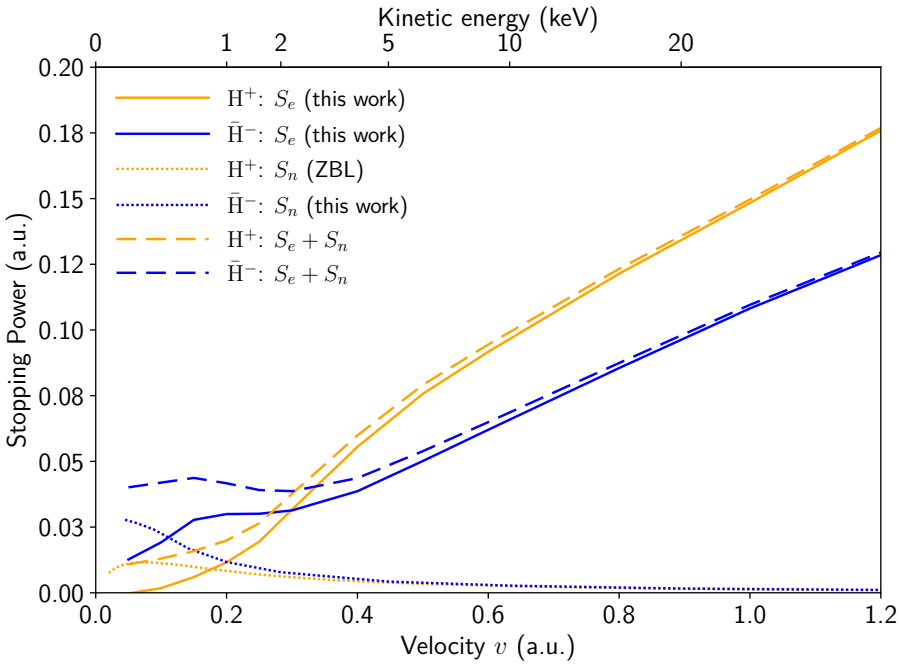

FIG. 6. Calculated electronic, nuclear, and total stopping power in LiF for protons and antiprotons.

B. Minimal approach distance

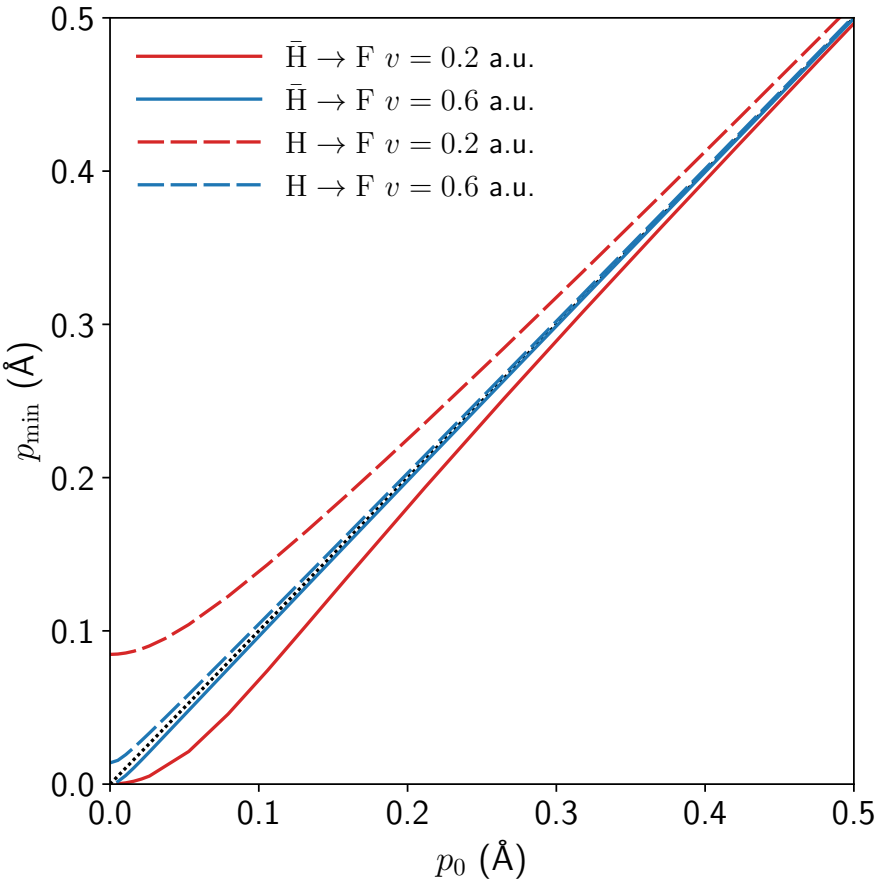

FIG. 7. Minimal distance p_{min} actually reached durgin the collision with a starting impact parameter p_0 for a proton or an antiproton colliding with a fluorine atom

The classical trajectories calculated above give also access to the actual minimal distance reached in a collision. In Fig. 7, we see that at $v = 0.6$ a.u., $p_{\mathrm{min}} \approx p_0$. we see the contrasted behavior behavior of protons and antiprotons. Therefore, the trajectories are very well approximated with straight-lines.

At lower velocity, $v = 0.2$ a.u., the trajectories become less rectilinear and p_{min} and p_0 differ to some extent.

For antiprotons, the interaction potential is attractive and $p_{\mathrm{min}} < p_0$. This means that the actual trajectories will come closer to the atomic nuclei and therefore will experience a slightly larger stopping power.

For protons, quite the contrary, the interaction potential is repulsive and $p_{\mathrm{min}} > p_0$. Then the actual trajectories will be repelled away from the atomic nuclei and therefore will experience a slightly lower stopping power.

However, the visible differences between p_{min} and p_0 only occur at very close encounter $p_0 < 0.1$ Å. These trajectories have a small weight in the impact parameter averaged stopping power (random stopping power). Those trajectories with $p_0 < 0.1$ Å accounts for about 1.5 % of the geometrical weight when performing the impact parameter average.

As a conclusion, considering the deviation from the straight-line trajectories may affect, but only slightly, the final result. Its effect, if any, would be to decrease the stopping power of protons and increase that of antiprotons. This again supports the existence of the negative Barkas coefficient in LiF at low velocity.

III. ELECTRONIC EXCITATIONS OF F^- ATOMIC TARGET FROM RT-TDDFT

The role of the different orbitals is qualitatively the same in real-time TDDFT (Fig. 8) and in linear-response TDDFT as presented in Fig. 4 of the Letter. From RT-TDDFT, one can define occupations p_i of a ground-state orbital i in the following manner:

$$p_i(t) = \sum_j f_j |\langle \varphi_i(t=0) | \varphi_j(t) \rangle|^2, \tag{6}$$

where f_j is an occupation of an electronic level j.

Fig. 8 represents the projection of the RT-TDDFT occupied orbitals on the initial orbitals for projectile velocities $v = 0.2$ a.u. and $v = 0.8$ a.u. Let us first consider the case of the low velocity, $v = 0.2$ a.u., at which the negative Barkas coefficient is observed (Fig. 8, panels a and b). As expected, for the proton, the electronic levels of F^- get minimally excited at such projectile velocities. For the antiproton, mostly the p_x and p_z orbitals get depopulated. In the main text, using the linear-response TDDFT, we show that the most unstable F^- orbital (named p_u) points towards the antiproton. As the F^- anion and the antiproton are contained in the xz-plane, a depopulation of those orbitals, p_x and p_z, is observed at the end of the RT-TDDFT simulation.

For the larger velocity, $v = 0.8$ a.u., there is no noticeable difference between the proton and the antiproton cases (Fig. 8, panels c and d). Furthermore, in contrast to the low-velocity case, the faster projectiles excite almost equally the $2s$, $2p_x$, $2p_y$, and $2p_z$ orbitals of F^- for both the proton and antiproton cases, which gives rise the more standard behavior.

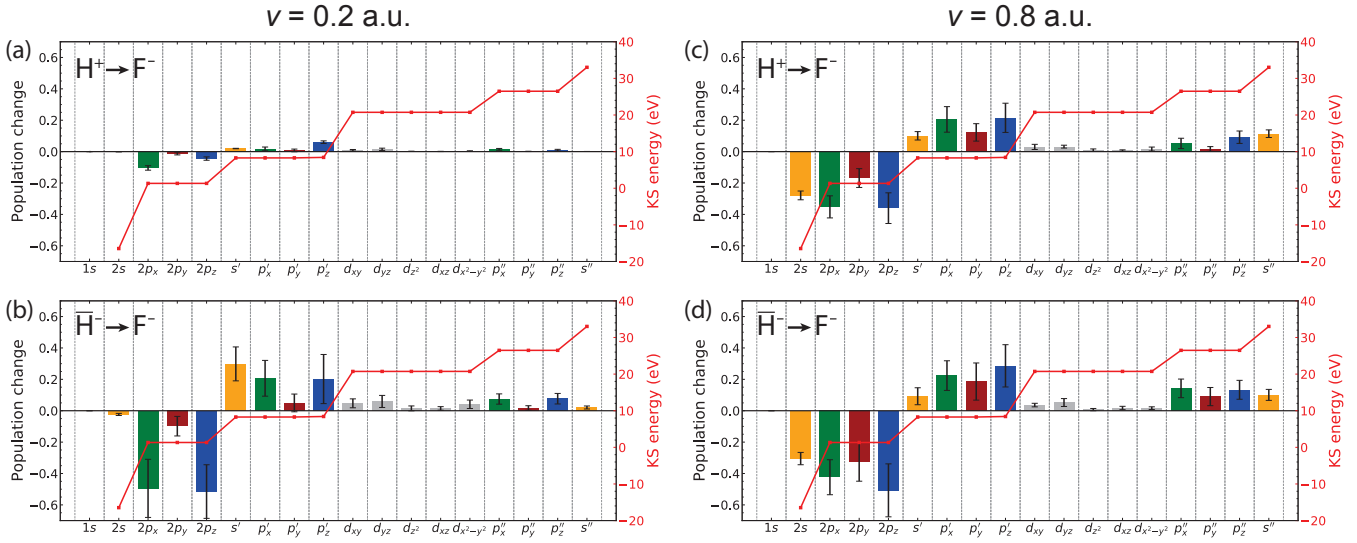

FIG. 8. Difference of the F^- electron orbital occupations after the collision with a proton at $v = 0.2$ a.u. (panel a), antiproton at $v = 0.2$ a.u. (panel b), proton at $v = 0.8$ a.u. (panel c), and antiproton at $v = 0.8$ a.u. (panel d). The differences are taken with respect to the initial occupation of states. The impact parameter for both projectiles is $p = 0.26$ Å. The error bars quantify the oscillation in time of the populations after the collision. The corresponding Kohn-Sham energies of the initial states are presented in red (right axes).

[1] I. Maliyov, J.-P. Crocombette, and F. Bruneval, The European Physical Journal B **91**, 172 (2018).
[2] K. G. Reeves, Y. Yao, and Y. Kanai, Phys. Rev. B **94**, 041108 (2016).
[3] C. Shepard, R. Zhou, D. C. Yost, Y. Yao, and Y. Kanai, J. Chem. Phys. **155**, 100901 (2021), https://doi.org/10.1063/5.0057587.
[4] P. Borlido, T. Aull, A. W. Huran, F. Tran, M. A. L. Marques, and S. Botti, J. Chem. Theory Comput. **15**, 5069 (2019), https://doi.org/10.1021/acs.jctc.9b00322.
[5] S. Refaely-Abramson, M. Jain, S. Sharifzadeh, J. B. Neaton, and L. Kronik, Phys. Rev. B **92**, 081204 (2015).
[6] A. A. Correa, Comput. Mater. Science **150**, 291 (2018).
[7] J. F. Ziegler, J. P. Biersack, and U. Littmark, *The stopping and ranges of ions in matter* (Pergamon, New York, 1985).
[8] J. F. Ziegler, M. Ziegler, and J. Biersack, Nucl. Instrum. Meth. B **268**, 1818 (2010), 19th International Conference on Ion Beam Analysis.
[9] K. Nordlund, D. Sundholm, P. Pyykkö, D. M. Zambrano, and F. Djurabekova, Phys. Rev. A **96**, 042717 (2017).
[10] F. Bruneval, T. Rangel, S. M. Hamed, M. Shao, C. Yang, and J. B. Neaton, Comput. Phys. Commun. **208**, 149 (2016).